Russian Journal of Earth Sciences

Dynamic, Chemical and Biological Features of the Southern Ocean Fronts in Austral Autumn 2024

A. V. Vesman[1,*], Y. V. Shved[1], D. A. Smirnova[2], A. A. Fedotova[2], A. A. Petrova[1], D. I. Frey[2]

[1] Arctic and Antarctic Research Institute, Otto Schmidt Laboratory for Polar and Marine Research, Saint-Petersburg, Russia
[2] Shirshov Institute of Oceanology, Russian Academy of Sciences, Moscow, Russia
* **Correspondence to:** Anna V. Vesman, anna.vesman@aari.ru

Abstract: This study provides a multidisciplinary analysis of the fronts and frontal zones along a 6,000 km transect in the Southern Ocean. Observations were carried out aboard the research vessel "*Akademik Tryoshnikov*" from April 2 to 13, 2024 on the way from Cape Town to Mirny wintering station and cover the waters of the Atlantic and Indian sectors of the Southern Ocean. Using satellite altimetry and shipboard data, we mapped the Antarctic Circumpolar Current (ACC) and its multi-branch structure, including the Subantarctic Front (SAF), Polar Front (PF), and Southern ACC Front (SACCF). Observations revealed dynamic interactions within the ACC, with the convergence of the PF branches producing strong southeastward flows, reaching 53 cm/s at the surface levels and decreasing to 26 cm/s at a depth of 550 m. Alongside physical measurements, nutrient and phytoplankton distributions were analyzed, highlighting sharp gradients in silica, phosphorus, and chlorophyll-*a* concentrations across fronts. In nutrient-rich zones such as the Polar Front and south of the ACC, diverse and abundant phytoplankton communities were observed, particularly diatoms such as *Fragilariopsis kerguelensis* and *Rhizosolenia simplex*. These findings show how combined use of biochemical and hydrodynamic data can contribute to better understanding of the complex structure of the ACC and surrounding waters.

Keywords: Southern Ocean, front, frontal zone, ACC, SADCP, altimetry data, nutrients, chlorophyll-*a*.

Citation: Vesman A. V., Shved Y. V., Smirnova D. A., Fedotova A. A., Petrova A. A., and Frey D. I. (2025), Dynamic, Chemical and Biological Features of the Southern Ocean Fronts in Austral Autumn 2024, *Russian Journal of Earth Sciences*, 25, ES5012, EDN: OKKQRQ, https://doi.org/10.2205/2025es001011

1. Introduction

The Antarctic Circumpolar Current (ACC) is the most powerful current, not only in the Southern Ocean but in the entire World Ocean. Traditionally, three jets and associated fronts are distinguished in the Southern Ocean: the Subantarctic Front (SAF), Polar Front (PF), and Southern ACC Front (SACCF) [*Burkov*, 1994; *Deacon*, 1982; *Orsi et al.*, 1995]. However, based on satellite altimetry, hydrographic and Argo data, several studies have suggested a more complex structure for the ACC. Recent research, however, has raised doubts about this interpretation. Several studies indicate that the frontal structure of the ACC rearranges multiple times around the circumpolar circuit [*Chapman*, 2017; *Chapman et al.*, 2020; *Graham et al.*, 2012; *Thompson et al.*, 2010]. It was shown that the splitting of a single front into multiple subfronts is observed, rather than the coherent meandering of individual frontal branches as suggested by previous studies [*Chapman*, 2014; *Chapman et al.*, 2020; *Langlais et al.*, 2011; *Orsi et al.*, 1995; *Sokolov and Rintoul*, 2009a,b; *Tarakanov and Gritsenko*, 2014]. For instance, in a study on the structure of the ACC south of Africa, 11 jets were identified within the current [*Tarakanov and Gritsenko*, 2014]. The northern boundary of the Southern Ocean is typically defined along the Subantarctic Front, which

Research Article

Received: December 23, 2024
Accepted: April 10, 2025
Published: October 9, 2025

also marks the northern boundary of the ACC [*Gille et al.*, 2016; *Rintoul et al.*, 2001; *Sokolov and Rintoul*, 2009b].

The presence of fronts in the Southern Ocean has significant implications for both the physical oceanography of the region and the broader climate system. For example, the strong density gradients near these fronts, driven by thermal wind, generate powerful oceanic jets. These frontal jets play a dominant role in the ACC transport and act as barriers to horizontal mixing: it is more challenging to move tracers across a jet than along the current [*Chapman and Sallée*, 2017; *Chapman et al.*, 2020; *Garabato et al.*, 2011; *Thompson and Sallée*, 2012]. Additionally, frontal regions are key sites of exchange between the deep and surface ocean, where both upwelling (the rising of deeper waters) and downwelling (the sinking of surface waters) are enhanced [*Chapman et al.*, 2020; *Stukel et al.*, 2017]. Fronts also help generate mesoscale eddies [*Chambers*, 2018; *Williams et al.*, 2007] and submesoscale filaments, which can bring nutrients from the deep ocean to the surface, where they become available for biological consumption [*Chapman et al.*, 2020; *d'Ovidio et al.*, 2010; *Lévy et al.*, 2018; *Morozov et al.*, 2022]. Chlorophyll concentrations follow these dynamic features, even at the scale of mesoscale eddies, a pattern that can partly be traced back to the upwelling of nutrients at many of the fronts [*Sokolov and Rintoul*, 2007].

Currently, definitions of fronts fall into two broad categories: local definitions and global definitions [*Chapman*, 2014]. Local definitions use criteria based on conditions in the immediate vicinity of a specific geographic location to determine whether a front is present. Locally defined fronts are not necessarily continuous, and their number can vary in space and time. Global definitions aim to identify a specific quantity – such as a particular value of temperature or SSH – that can be used to detect a front over a defined region, or even across the entire ACC [*Sokolov and Rintoul*, 2007]. Fronts defined using global criteria are typically continuous in space, and the number of fronts is chosen a priori [*Langlais et al.*, 2011]. Recent studies do not suggest that any single front is observed as a continuous structure across the entire ACC [*Chapman*, 2017; *Graham et al.*, 2012; *Thompson et al.*, 2010]. However, organizing these narrow, discontinuous jets into distinct ACC fronts remains a useful approach for understanding the distribution of nutrient properties and the cross-front exchange of these nutrients [*Barré et al.*, 2011].

The primary objective of this study was to characterize the hydrodynamic and hydrochemical properties of the waters south of Africa during the austral autumn of 2024. Specifically, this work aimed to: (1) identify the locations of the main fronts and jets based on the widely accepted classification of the Southern Ocean fronts [*Palter et al.*, 2013; *Sokolov and Rintoul*, 2009a,b], and (2) describe the key characteristics of these fronts.

2. Data and Methods

A comprehensive study of fronts and frontal zones of the Southern Ocean was performed along a distance of more than 6,000 km aboard the research vessel (R/V) "*Akademik Tryoshnikov*" from April 2 to 13, 2024. The data collected along the ship track from Cape Town to Mirny station was divided into two sections: quasi-meridional (40–57.31°S), including stations 1–63, and quasi-zonal (18–90°E), which includes stations 64–94 (Figure 1, Figure 2).

2.1. In-situ Temperature Data

In this study, along-track temperature measurements were collected using the internal sensor of the Shipborne Acoustic Doppler Current Profiler (SADCP) Teledyne RD Instruments Ocean Surveyor 75 kHz. These data allow us to analyze the temperature distribution along the entire ship track. The values collected using the SADCP were compared to manual measurements taken by the WTW Multi 3420 multiparameter meter, which were simultaneously recorded during hydrochemical and biological sampling, as well as with thermometer measurements taken every 3 hours. It was found that the temperature values from the SADCP were overestimated. However, since temperature measurements are used as an auxiliary parameter, primarily for analyzing gradients, this dataset is presented

uncorrected. For biochemical analysis, the simultaneous manual measurements by the WTW Multi 3420 multiparameter meter are used as a supplementary dataset.

2.2. Shipborne ADCP Measurements

The direct velocity measurements were carried out using the SADCP Teledyne RD Instruments Ocean Surveyor with a frequency of 76.8 kHz (TRDI OS75), installed onboard the R/V *"Akademik Tryoshnikov"*. Measurements were conducted in narrowband mode to a depth of 700 m. The quality of the data depended on weather and ice conditions. We set the standard quality criteria ("Percent good") at 50%. The true heading was obtained from the Inertial Navigation System (INS) Hydrins [*Exail*, 2025]. The bin size was 16 m, with an 8 m blank distance immediately below the transducer. The ship's draught is 8.5 m, so the depth of the first bin center is 32.5 m. According to technical protocols, the near-bottom layer was excluded, with its thickness set to 15% of the ocean depth. The upper 70 m layer was also removed due to incorrect data. The time average interval for raw data was 120 s; at the mean ship speed of 13 knots, this interval corresponds to 800 m of along-track averaging. Measurement errors in the amplitudes of horizontal velocities using the described method do not exceed 2 cm/s [*Chereskin and Harris*, 1997; *Frey et al.*, 2021]. Simultaneous barotropic tidal velocities were calculated using the TPXO model version 9.1 [*Egbert and Erofeeva*, 2002]. Direct velocity observations were corrected using these modeled tidal velocities.

2.3. Satellite Altimetry Data

Altimetry-derived mapped data on absolute dynamic topography (ADT) and geostrophic velocities from CMEMS (Copernicus Marine Environment Monitoring Service, product SEALEV-EL_GLO_PHY_L4_MY_008_047) [*European Union-Copernicus Marine Service*, 2021] were used to determine the positions of the fronts. This product includes data from all available altimeters and provides maps of surface geostrophic circulation and sea level with a spatial resolution of 0.25° on a regular grid and daily sampling [*Pujol et al.*, 2016]. The satellite revisit time is approximately 9.9 days or longer, depending on the platform. As a result, velocity fluctuations shorter than about 20 days are not adequately captured by altimetry-derived products [*Artana et al.*, 2018; *Frey et al.*, 2023]. Therefore, satellite-derived geostrophic velocity shows a significant correlation with in-situ observations only after applying a 20-day low-pass filter [*Ferrari et al.*, 2017]. The altimetric mapping process tends to smooth out fronts and reduce the velocities of associated currents [*Frey and Kubryakov*, 2023]. Despite these limitations, the use of altimetry data allows for the study of ocean circulation with consistent temporal and spatial resolution, providing context for the results of single transects both in time and space.

2.4. Chemical and Biological Data

All hydrochemical samples were collected along the ship track from the sea surface by a bucket. If the weather conditions prevented direct sampling from open decks, samples were collected from the flow-through system. Intercomparison of results obtained by these two methods showed that they are in a good agreement and can be analyzed together. All samples were processed within a few hours of collection in the ship's hydrochemical laboratory.

The content of dissolved inorganic phosphorus (PO_4) in seawater was determined using a modified Murphy-Riley method [*Guide...*, 2003; *Murphy and Riley*, 1958]. The method is based on the formation of a molybdenum blue complex from the reaction of orthophosphate and ammonium molybdate in the presence of sulfuric acid and potassium antimony tartrate, which, when reduced with ascorbic acid, forms the blue complex. The color intensity of the molybdenum blue complex is proportional to the phosphate content in the solution. Optical density was measured at a wavelength of 885 nm.

The mass concentration of dissolved inorganic silicon (SiO_3) was determined by the photometric method, which is based on the interaction of monomeric-dimeric forms of

silicon with ammonium molybdate in an acidic medium. This reaction forms a silicon-molybdenum complex, which, when reduced with ascorbic acid, yields a blue-colored form. The maximum absorption of the resulting compound is observed at 810 nm [*Guide...*, 2003; *Intergovernmental Oceanographic Commission*, 1983].

Chlorophyll-*a* concentration was determined using the fluorometric method [*Arar and Collins*, 1997]. A 1-liter water sample was filtered through a GF/F glass fiber filter 47 mm with a pore size of 0.7 μm. Chlorophyll-*a* was extracted from the filter with a 90% acetone solution (5 mL) for 30 minutes in a dark, cool place.

Phytoplankton samples were collected along the ship track by filtering a set volume of water (10 liters) through a small Juday net with a mesh size of 20 μm and were concentrated in a glass container to 60 mL. Lugol's solution was used as a fixative. All samples were stored in a dark place in a refrigerator. For further determination of the species composition, the samples were delivered to the laboratory and analyzed under a light microscope. The biomass of phytoplankton was calculated using the counting-weight method. This method involves determining the volume of algae cells, where the shape of the cell is approximated to the closest geometric figure, and the volume of the cell is calculated using stereometric formulas [*Karlson et al.*, 2010; *Sun and Liu*, 2003]. In this case, the density of phytoplankton is assumed to be one. Mass species of algae typically have shapes such as spheres, cylinders, or ellipsoids. To calculate the biomass, the average volume of the organism for each species is multiplied by the number of organisms of that species.

3. Results and Discussion

3.1. Dynamic Structure of ACC Branches (Quasi-Meridional Section)

In this study, we use the generally accepted classification of the Southern Ocean fronts [*Barré et al.*, 2011; *Sokolov and Rintoul*, 2009a,b]. These fronts or branches, from north to south, are: two branches of the Subantarctic Front (SAF)—SAF-N (north) and SAF-M (middle); three branches of the Polar Front (PF)—PF-N (north), PF-M (middle), and PF-S (south); two branches of the Southern ACC Front (SACCF)—SACCF-N (north) and SACCF-S (south); and the southern boundary (SB) of the ACC. We determine the location of these fronts based on satellite altimetry data. We use the criteria suggested by *Barré et al.* [2011], where the largest ADT gradient amplitudes associated with the fronts are located at the ADT contours: 23 cm (SAF-N), −10 cm (SAF-M), −43 cm (PF-N), −62 cm (PF-M), −79 cm (PF-S), −93 cm (SACCF-N), −104 cm (SACCF-S), and −114 cm (SB).

The 23 cm ADT isoline usually associated with the SAF-N front was crossed south of Africa several times (dark purple line in Figure 1). Satellite altimetry data suggest that these ADT variations are caused by mesoscale eddies. In-situ temperature data along the track confirm this hypothesis; temperature changes caused by crossing of the SAF are higher than during crossing individual eddies (black line in Figure 1(d)). These eddies are filled with subtropical waters and usually observed in this region. The northern branch of the Subantarctic Front (SAF-N) was crossed on 3 April 2024. A jet with a maximum velocity of 51 cm/s at a depth of 105 m directed to the southeast was observed at the intersection with the SAF-N front between station 4 and 5. Velocity values of 20 cm/s were recorded at a depth of 330 m. The middle branch of the Subantarctic Front (SAF-M) was crossed on April 4, 2024 between station 10 and 11 (Figure 1). A weak ACC jet was observed at this crossing based on the SADCP data. The maximum recorded velocity was 21 cm/s at a depth of 90 m.

The branches of the Polar Front were closest to each other during ship observations on April 4 and 5, 2024 (Figure 1). The northern branch of the Polar Front (PF-N) was crossed in the area of station 17 at 49.25°S. According to SADCP data, a wide and deep jet of predominantly southern direction with maximum velocities of up to 36 cm/s at a depth of 280 m was recorded from 48° to 49.1°S. At a depth of 540 m, velocities of 28 cm/s were observed in this area. The middle branch of the Polar Front (PF-M) was crossed at 50.2°S on April 5, 2024, between stations 22 and 23 (Figure 1). On the same day, at 50.6°S, the southern branch of the Polar Front (PF-S) was crossed in the area of station 25. The

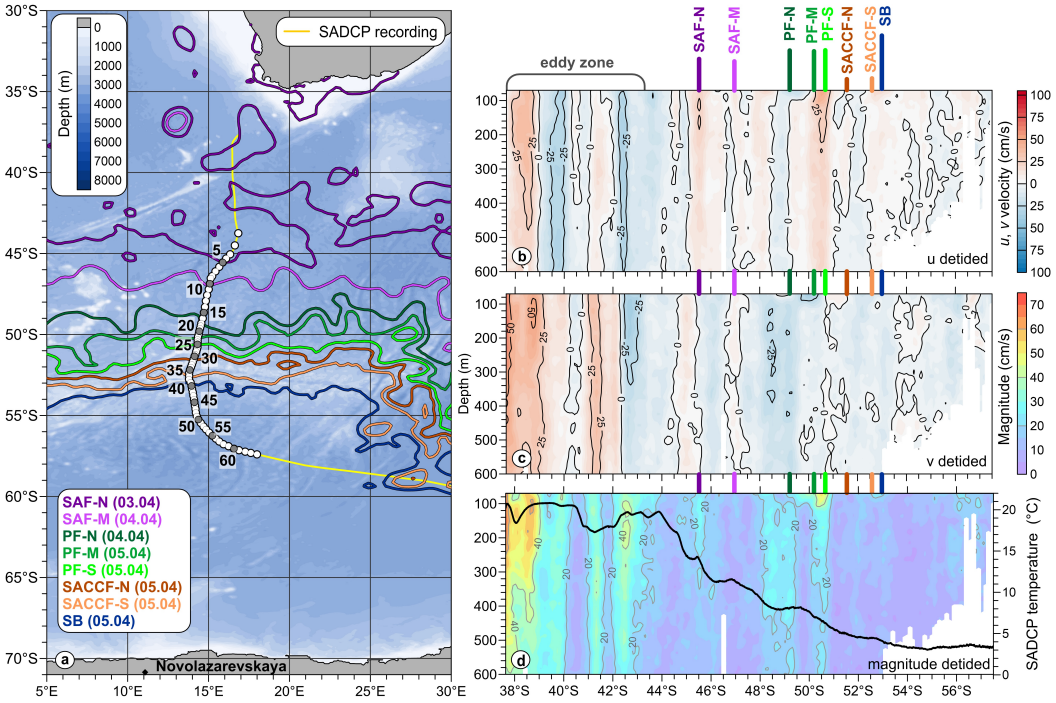

Figure 1. Position of the Southern Ocean fronts based on satellite altimetry data (a) and continuous measurements of current velocity at the quasi-meridional section: zonal component *u* with tide correction (b), meridional component *v* with tide correction (c) and velocity magnitude with tide correction (d). The positions of the fronts are given based on the absolute dynamic topography values according to [*Barré et al.*, 2011]. The fronts are (from north to south): dark purple line – the northern branch of the Subantarctic Front (SAF-N), light purple – the middle branch of the Subantarctic Front (SAF-M), dark green – the northern branch of the Polar Front (PF-N), green – the middle branch of the Polar Front (PF-M), light green – the southern branch of the Polar Front (PF-S), red – the northern branch of the Southern Front of the ACC (SACCF-N), orange – the southern branch of the Southern Front of the ACC (SACCF-S), black – the southern boundary of ACC (SB). The yellow line shows the area of associated measurements. White circles indicate stations where surface water samples were collected. The station numbers are shown in panel (a). The bottom topography is taken from the GEBCO 2022 database [*GEBCO Bathymetric Compilation Group 2022*, 2022]. In panel (d), the black line represents the subsurface temperature from the internal SADCP sensor. The colored lines above panels (b–d), show the position of the fronts according to the legend.

fronts were located so close to each other that they appeared as a single stream directed southeast, based on the SADCP data. The highest current velocities among all branches of the Antarctic Circumpolar Current fronts were recorded here. Velocities reached 53 cm/s at a depth of 70 m. These high velocities are most likely caused by the convergence of the PF branches. Velocities of more than 26 cm/s were observed down to a depth of 550 m. A current with velocities of up to 42 cm/s was observed between PF-N and PF-S in the upper 100-meter layer. This is probably the result of the interaction of the three branches of the Polar Front. The northern branch of the Southern ACC Front (SACCF-N) on the quasi-meridional section of the route was crossed on April 5, 2024, in the area of station 31 at 51.5°S. Like the SAF-M, this branch was not clearly observed based on the SADCP data. The velocity values in this area did not exceed 15 cm/s. The southern branch of the Southern ACC Front (SACCF-S) was crossed on April 6, 2024, at 52.6°S near station 37, between 51.75° and 53.3°S. Velocities of more than 20 cm/s were recorded in the upper 85-meter layer and at depths down to 500 m. The highest velocity values of 24 cm/s were observed at a depth of 70 m. Two narrow flows with velocities of up to 21 cm/s were identified in the upper 330 m layer.

3.2. Dynamic Structure of Currents South of ACC (Quasi-Zonal Section).

The quasi-zonal section was located along the southern boundary of the ACC (SB) in the Indian sector of the Southern Ocean (from 18° to 90°E). Measurements along this section were performed from 6 to 13 April 2024. Two meanders of the SACCF were crossed in the area of station 80 (36.85°E) and station 84 (51.76°E). Additionally, two eddies were crossed near stations 75 (27.39°E) and 77 (30.49°E) (Figure 2).

The maximum velocities were recorded in one of the eddies at 26.6°E, where the velocities reached 66 cm/s at a depth of 180 m (Figure 2). The current was directed southwest. High velocities (up to 53 cm/s) were observed down to a depth of 350 m. At 29.3°E, another well-defined jet directed southwest was observed. The maximum velocity of 52 cm/s was measured at a depth of 250 m, with values exceeding 30 cm/s at a depth of 500 m. In addition, a southward jet was recorded at 35°E. The velocity of jets at 41.4° and 46.7°E reached 47 cm/s and was directed southeast. At 75°E, a northeastward current was observed with a maximum velocity of 67 cm/s at a depth of 75 m.

3.3. Chemical and Biological Features

According to hydrobiological parameters, sampling began near the Subtropical Front, which was characterized by a chlorophyll-*a* concentration of 0.53 mg/m^3 (point 1, Figure 3), a sharp increase in phosphates (from 0.1 μM to 0.4 μM), and a decrease in seawater temperature (from 20 °C to 15 °C). The species diversity of phytoplankton is mainly represented by the diatoms *Fragilariopsis kerguelensis* and the genus *Rhizosolenia sp.*, as well as single cells of the genera *Pseudo-nitzschia sp.*, *Cylindrotheca sp.*, *Actinocyclus sp.*, *Thalassionema sp.*, and the dinoflagellate *Tripos furca*.

At the approach of the Subantarctic Zone, chlorophyll-*a* values slowly decreased to 0.15 mg/m^3. In the biogeochemical structure, the SAF is distinguished by a sharp increase in the concentrations of phosphates and nitrates, as well as a sharp decrease in water temperature in the surface layer [*Artamonova et al.*, 2021]. Around 47.2–47.9°S, the sea surface temperature decreased by about 2 °C, and PO_4 concentrations increased from 0.97 to 1.23 μM. In [*Artamonova et al.*, 2021], based on several years of observations, it is noted that an increase in SiO_3 associated with the SAF is observed in some years but not always. During this campaign, the increase in silicates was not substantial (from near zero to 1.96 μM). The chlorophyll-*a* values increased to 0.32 mg/m^3.

To the south of the SAF, two major zones in the Southern Ocean can be separated: the Subantarctic, which is poorer in nutrients, and the Antarctic, which has high concentrations of nutrients. These two zones are separated by a clearly defined hydrochemical front [*Artamonova et al.*, 2021; *Batrak*, 2008; *Maslennikov*, 2004]. The interaction of Subantarctic and Antarctic waters occurs in the South Polar Frontal Zone (SPFZ), which has the Subantarctic Front (SAF) as a boundary to the north and the Southern Polar Front (SPF) to the south. This year, the SPFZ was characterized by a steady increase in phosphorus concentrations, low concentrations of silicates (around 1.5 μM), and a decrease in chlorophyll-*a* concentrations to 0.21 mg/m^3. The species diversity is represented mainly by dinoflagellate algae of the genera *Ceratium sp.*, *Gymnodinium sp.*, *Protoperidinium sp.*, while diatoms of the species *Fragilariopsis kerguelensis* were also found.

In the SPF area, a surface gradient of dissolved inorganic silicon was observed, with its concentration sharply increasing from 1.5 to 17.35 μM. The SPF is the boundary beyond which the total bioproductivity of the waters begins to gradually increase. South of the SPF, a belt of the ACC was observed: phosphorus concentrations did not exceed 1.51 μM, silica concentrations increased to 19.58 μM, chlorophyll-*a* concentrations rose from 0.25 mg/m^3 to 0.78 mg/m^3, and biomass increased accordingly from 6 mg/m^3 to 158 mg/m^3. Preliminary analysis of the phytoplankton community in the ACC zone showed a fairly high diversity of microalgae and their large cell size. During the analysis of the samples, a large number of diatoms, including *Rhizosolenia honetata*, *Rhizosolenia simplex*, *Fragilariopsis kerguelensis*, *Chaetoceros atlanticus f. bulbosum*, *Thalassiothrix antarctica*, *Corethron pennatum*, *Corethron inerme*, *Guinardia cylindrus*, and single cells of *Leptocylindrus mediterraneus*, *Pro-*

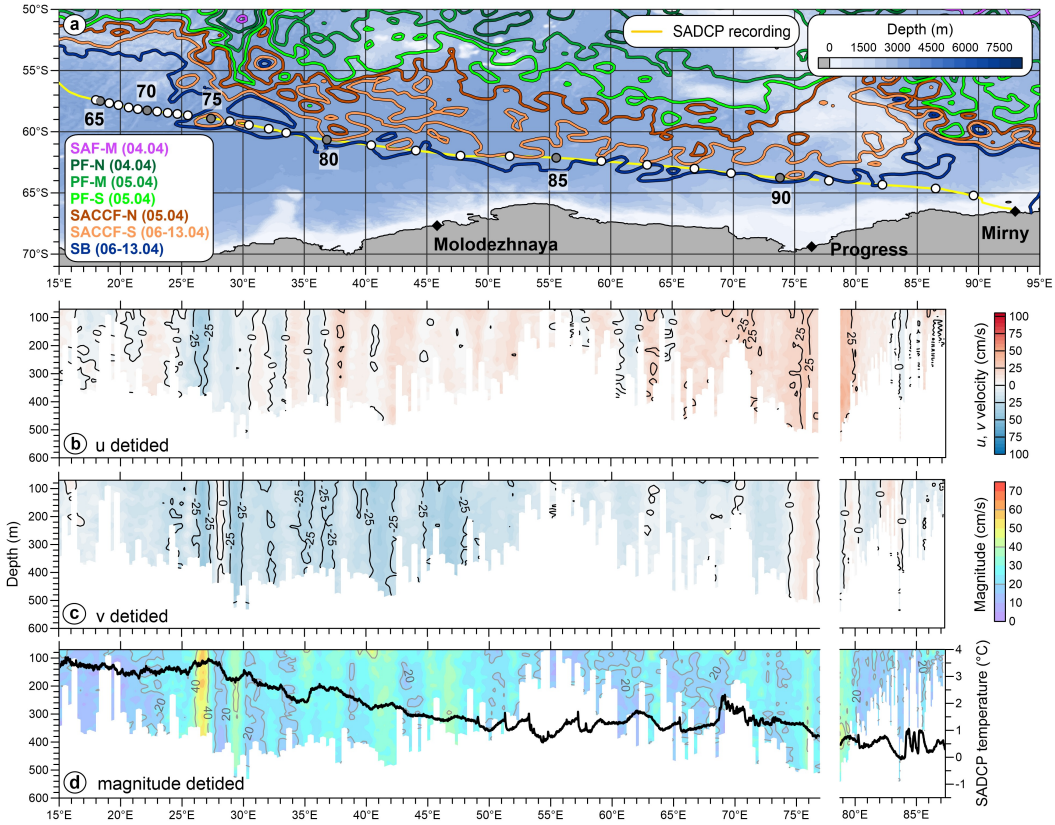

Figure 2. Position of the Southern Ocean fronts based on satellite altimetry data (a) and continuous measurements of current velocity in the quasi-zonal region: zonal component *u* with tide correction (b), meridional component *v* with tide correction (c) and magnitude with tide correction (d). The positions of the fronts are given based on the absolute dynamic topography values according to [*Barré et al.*, 2011]. The fronts are (from north to south) dark purple line – the northern branch of the Subantarctic Front (SAF-N), light purple – the middle branch of the Subantarctic Front (SAF-M), dark green – the northern branch of the Polar Front (PF-N), green – the middle branch of the Polar Front (PF-M), light green – the southern branch of the Polar Front (PF-S), red – the northern branch of the Southern Front of the ACC (SACCF-N), orange – the southern branch of the Southern Front of the ACC (SACCF-S), black – the southern boundary of ACC (SB). The yellow line shows the track with continuous measurements. White circles indicate stations where surface water samples were collected. The numbers indicate the station number. The bottom topography is taken from the GEBCO 2022 database [*GEBCO Bathymetric Compilation Group 2022*, 2022]. In panel (d), the black line represents corrected temperature from the internal SADCP sensor. The colored lines above panels (b–d), show the position of the fronts according to the legend.

boscia alata, as well as diatoms of the genera *Nitzschia sp.*, *Pseudo-nitzschia sp.*, *Coscinodiscus sp.*, *Chaetoceros sp.*, and *Asteromphalus sp.*, were found. These are the main consumers of silicon for the structure of their skeletons (shells), which can potentially explain the observed sharp decrease in silica concentrations.

Within the Antarctic zone, there is the Southern ACC Front (SACCF) [*Orsi et al.*, 1995], also known as the Secondary Frontal Zone of Antarctica [*Bogdanov et al.*, 1986; *Fedulov and Shnar*, 1990; *Maslennikov*, 2004; *Maslennikov and Popkov*, 1988]. This front is formed between two structural modifications of Antarctic-type waters and separates the waters of the southern periphery of the ACC from the waters of the high-latitude modification, which are confined to the continental cyclonic gyres [*Maslennikov*, 2004]. In the SACCF area, a sharp gradient in the concentration of SiO_3 is observed, which serves as a surface criterion for identifying this front [*Arzhanova and Artamonova*, 2014; *Batrak*, 2008; *Franck et al.*, 2000]. During observations silica concentrations increased up to 40.51 μM. Another

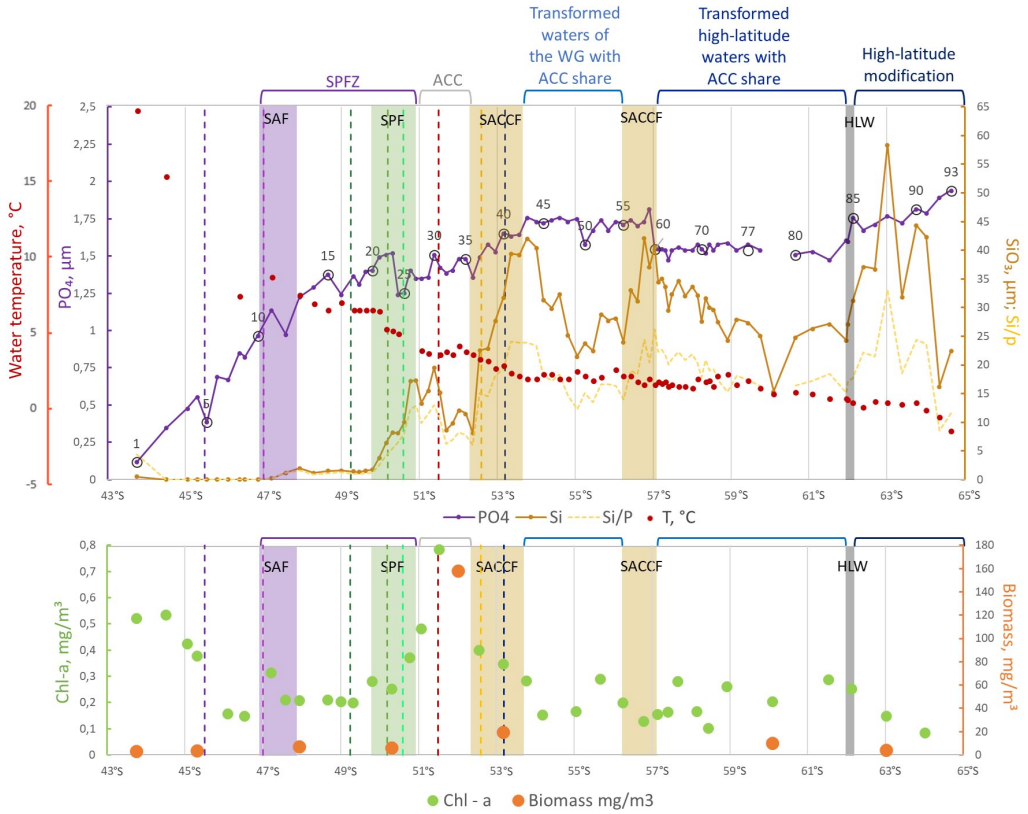

Figure 3. Surface distribution of nutrients: PO_4 (µM), SiO_3 (µM), Si to P ratio, water temperature and biological characteristics: chlorophyll-*a* concentration (mg/m^3) and phytoplankton biomass (mg of wet weight/m^3); colored dashed vertical lines correspond to the fronts defined by the dynamic parameters; colored boxes define frontal zones defined by biochemical parameters; black circles with numbers show station number.

good indicator of the SACCF is the Si/P ratio, which was about 24 [*Artamonova et al.*, 2021]. Chlorophyll-*a* values decrease, and at point 40, the concentration of chlorophyll-*a* reaches 0.40 mg/m^3. The nature of the silicon distribution is primarily determined by large-scale circulation features, while the distribution of mineral phosphorus is characterized by some mosaicism, which is associated with the intensity of photosynthesis [*Batrak*, 2008]. The composition of the phytoplankton community is dominated by typical representatives of Antarctic waters, such as diatoms of the species *Fragilariopsis kerguelensis*, *Thalassiothrix antarctica*, *Corethron pennatum*, and *Rhizosolenia simplex*.

On some years, to the south of the SACCF, the massif of waters from the eastern periphery of the Weddell Gyre (WG) is observed. Its defining feature is high concentrations of all nutrients, especially silica (45.7–80 µM) [*Artamonova et al.*, 2021]. However, no such concentrations were observed this year. On the contrary, the concentrations of silica and chlorophyll-*a* decreased to 21.55 µM and 0.17–0.29 mg/m^3, respectively. The Si/P ratio was around 15, which corresponds to the transformed waters formed by the return flow of the WG with a share of the ACC waters [*Artamonova et al.*, 2021]. At 56.24°S, a sharp increase in silica was observed (up to 42.21 µM), indicating that the second branch of the SACCF was crossed. This change was followed by a subsequent decrease in nutrient concentrations, likely associated with the transformed high-latitude waters with ACC share (PO_4 to about 1.54 µM; SiO_3 to about 24.85 µM, with the lowest concentration of 15.38 µM; Si/P around 16–17). The chlorophyll-*a* concentrations fluctuated between 0.1 and 0.28 mg/m^3.

The southern boundary of the ACC can be placed at 62°S. To the south of this, the waters of the high-latitude modification were observed, with high concentrations of both

phosphorus and silica and a decline in chlorophyll-*a* concentrations. The species diversity is represented mainly by diatoms of the genus *Coscinodiscus sp.*, *Actinocyclus sp.*, *Haslea sp.*, *Corethron sp.*, *Navicula sp.*, and the species *Proboscia alata*, *Proboscia inermis*, *Dactyliosolen antarctica*, *Fragilariopsis kerguelensis*, *Asteromphalus parvulus*, *Chaetoceros atlanticus f. bulbosum*, *Octactis speculum*, and *Eucampia antarctica*.

4. Conclusions

In this study, the global criteria were used for the analysis of dynamic structure, while the methodology for defining hydrochemical fronts leaned more toward local methods. This distinction leads to a slight discrepancy in the defined position of some frontal zones (Figure 3). However, combined use of satellite data, hydrodynamical in-situ data and biochemical data allows us to comprehensively describe features and position of each frontal zone. Despite the fact that SADCP data show increase in *u* current speed component associated with the SAF, PF, SACCF and SB sometimes it is difficult to identify each frontal zone based solely on dynamic data as these observations are complex and lack clarity without additional information. Hydrochemical observations help to solve this problem since there are established changes in parameters that correspond to each frontal zone. At the same time both of these data types add important information for understanding changes in water masses observed in the study region.

The collected SADCP data provide direct estimates of the ACC branches kinematic structure. It was confirmed that the maximum velocity of the branches depends on the convergence and merging of separate ACC jets. The measured vertical structures of the branches are barotropic; the highest current velocities among all branches of the Antarctic Circumpolar Current fronts were recorded along the Polar Front. The maximum observed velocities were 51 cm/s (Subantarctic Front), 53 cm/s (Polar Front), and 24 cm/s (Southern ACC Front). The maximum velocity is usually observed at a depth around 100 m.

Phosphates concentrations increased progressively from the STF (0.4 μM) to the Antarctic Zone (>1.5 μM), reflecting the nutrient enrichment typical of high-latitude waters. Dissolved inorganic silicon concentrations exhibited sharp gradients, particularly at the SPF and SACCF, where levels increased from 1.5 μM to 17.35 μM and from about 9 μM over 40 μM, respectively. Varied between zones, highlighting differences in nutrient cycling. The SACCF showed a high Si/P ratio (~24), indicating silicate-rich waters, while regions south of the SACCF displayed lower ratios (15–17), reflective of nutrient transformation and utilization.

Chlorophyll-*a* concentrations, serving as a proxy for primary productivity, fluctuated across the zones. Higher concentrations (up to 0.78 mg/m^3) were observed in the ACC and near the STF, aligning with increased nutrient availability. In contrast, chlorophyll-*a* levels declined south of the SACCF, suggesting reduced productivity despite nutrient abundance, likely due to seasonal factors. Phytoplankton species diversity was predominantly represented by diatoms. An exception was noted in the SAF zone, which was dominated to a greater extent by dinophyte algae, including genera *Ceratium*, *Gymnodinium*, and *Protoperidinium*. The most common diatom species was *Fragilariopsis kerguelensis*, along with numerous cells from the genera *Rhizosolenia*, *Pseudo-nitzschia*, and *Chaetoceros*.

Acknowledgements. Authors are sincerely grateful to the Russian Antarctic expedition (RAE) for the opportunity to carry out research and the crew of the R/V *"Akademik Tryoshnikov"* and expedition members of the 69th RAE for their help. The authors are grateful to R. Yu. Tarakanov for valuable comments to the article. The study was carried out within state task no. FMWE-2024-0016 (analysis of satellite altimetry data) and the Russian Science Foundation, grant 22-77-10004 (analysis of SADCP measurements). Collection of hydrochemical and hydrobiological data was carried out in framework of project 5.2 "Oceanological, climatological, glaciological and geophysical research in Antarctica and the Southern Ocean" funded by Roshydromet of the Russian Federation.

References

Arar E. J. and Collins G. B. Method 445.0 In Vitro Determination of Chlorophyll a and Pheophytin a in Marine and Freshwater Algae by Fluorescence. — National Exposure Research Laboratory, Office of Research, Development, U.S. Environmental Protection Agency, 1997. — 22 p.

Artamonova K. V., Gangnus I. A., Dukhova L. A., et al. Spatial hydrochemical structure in surface waters of the Southern ocean between Africa and Antarctica // Arctic and Antarctic Research. — 2021. — Vol. 67, no. 4. — P. 328–347. — https://doi.org/10.30758/0555-2648-2021-67-4-328-347. — (In Russian).

Artana C., Lellouche J. M., Park Y. H., et al. Fronts of the Malvinas Current System: Surface and Subsurface Expressions Revealed by Satellite Altimetry, Argo Floats, and Mercator Operational Model Outputs // Journal of Geophysical Research: Oceans. — 2018. — Vol. 123, no. 8. — P. 5261–5285. — https://doi.org/10.1029/2018jc013887.

Arzhanova N. V. and Artamonova K. V. Hydrochemical Structure of Water Masses in Areas of the Antarctic Krill (Euphausia Superba Dana) Fisheries // Trudy VNIRO. — 2014. — Vol. 152. — P. 118–132. — EDN: TGTNWF ; (in Russian).

Barré N., Provost C., Renault A., et al. Fronts, meanders and eddies in Drake Passage during the ANT-XXIII/3 cruise in January-February 2006: A satellite perspective // Deep Sea Research Part II: Topical Studies in Oceanography. — 2011. — Vol. 58, no. 25/26. — P. 2533–2554. — https://doi.org/10.1016/j.dsr2.2011.01.003.

Batrak K. V. Hydrochemical characteristic of different modifications of Antarctic waters // Oceanology. — 2008. — Vol. 48, no. 3. — P. 349–356. — https://doi.org/10.1134/S0001437008030065.

Bogdanov M. A., Makarov R. R., Maslennikov V. V., et al. The structure of hydrophysical fields in the Atlantic sector of the Southern ocean and their impact on plankton communities. — Moscow : ONTI VNIRO, 1986. — 64 p.

Burkov V. A. Antarctic jets // Oceanology of the Russian Academy of Sciences. — 1994. — Vol. 34, no. 2. — P. 145–153.

Chambers D. P. Using kinetic energy measurements from altimetry to detect shifts in the positions of fronts in the Southern Ocean // Ocean Science. — 2018. — Vol. 14, no. 1. — P. 105–116. — https://doi.org/10.5194/os-14-105-2018.

Chapman C. and Sallée J. B. Isopycnal Mixing Suppression by the Antarctic Circumpolar Current and the Southern Ocean Meridional Overturning Circulation // Journal of Physical Oceanography. — 2017. — Vol. 47, no. 8. — P. 2023–2045. — https://doi.org/10.1175/jpo-d-16-0263.1.

Chapman C. C. Southern Ocean jets and how to find them: Improving and comparing common jet detection methods // Journal of Geophysical Research: Oceans. — 2014. — Vol. 119, no. 7. — P. 4318–4339. — https://doi.org/10.1002/2014JC009810.

Chapman C. C. New Perspectives on Frontal Variability in the Southern Ocean // Journal of Physical Oceanography. — 2017. — Vol. 47, no. 5. — P. 1151–1168. — https://doi.org/10.1175/JPO-D-16-0222.1.

Chapman C. C., Lea M. A., Meyer A., et al. Defining Southern Ocean fronts and their influence on biological and physical processes in a changing climate // Nature Climate Change. — 2020. — Vol. 10, no. 3. — P. 209–219. — https://doi.org/10.1038/s41558-020-0705-4.

Chereskin T. K. and Harris C. L. Shipboard acoustic Doppler current profiling during the WOCE Indian Ocean expedition: I10. — Scripps Institution of Oceanography, University of California, San Diego, 1997. — 137 p.

d'Ovidio F., Monte S. De, Alvain S., et al. Fluid dynamical niches of phytoplankton types // Proceedings of the National Academy of Sciences. — 2010. — Vol. 107, no. 43. — P. 18366–18370. — https://doi.org/10.1073/pnas.1004620107.

Deacon G. E. R. Physical and biological zonation in the Southern Ocean // Deep Sea Research Part A. Oceanographic Research Papers. — 1982. — Vol. 29, no. 1. — P. 1–15. — https://doi.org/10.1016/0198-0149(82)90058-9.

Egbert G. D. and Erofeeva S. Y. Efficient Inverse Modeling of Barotropic Ocean Tides // Journal of Atmospheric and Oceanic Technology. — 2002. — Vol. 19, no. 2. — P. 183–204. — https://doi.org/10.1175/1520-0426(2002)019<0183:eimobo>2.0.co;2.

European Union-Copernicus Marine Service. Global Ocean Gridded L4 Sea Surface Heights and Derived Variables Reprocessed (1993-Ongoing). — 2021. — https://doi.org/10.48670/MOI-00148.

Exail. Inertial Navigation System (INS) Hydrins. — URL: https://www.ixblue.com/store/hydrins-2/ (visited on 02/03/2025).

Fedulov P. P. and Shnar V. N. Frontal zone and water structure of the Weddell Circle // Researches of the Weddell Circle. Oceanographic conditions and features of the plankton communities development. Digest of scientific papers. — Moscow : VNIRO, 1990. — P. 31–48. — (In Russian).

Ferrari R., Artana C., Saraceno M., et al. Satellite Altimetry and Current-Meter Velocities in the Malvinas Current at 41°S: Comparisons and Modes of Variations // Journal of Geophysical Research: Oceans. — 2017. — Vol. 122, no. 12. — P. 9572–9590. — https://doi.org/10.1002/2017jc013340.

Franck V. M., Brzezinski M. A., Coale K. H., et al. Iron and silicic acid concentrations regulate Si uptake north and south of the Polar Frontal Zone in the Pacific Sector of the Southern Ocean // Deep Sea Research Part II: Topical Studies in Oceanography. — 2000. — Vol. 47, no. 15/16. — P. 3315–3338. — https://doi.org/10.1016/s0967-0645(00)00070-9.

Frey D., Krechik V., Gordey A., et al. Austral summer circulation in the Bransfield Strait based on SADCP measurements and satellite altimetry // Frontiers in Marine Science. — 2023. — Vol. 10. — https://doi.org/10.3389/fmars.2023.1111541.

Frey D. I. and Kubryakov A. A. Dynamic Structure of Eddies of the Brazil-Malvinas Confluence Zone Revealed by Direct Measurements and Satellite Altimetry // Journal of Geophysical Research: Oceans. — 2023. — Vol. 128, no. 11. — https://doi.org/10.1029/2023jc019957.

Frey D. I., Piola A. R., Krechik V. A., et al. Direct Measurements of the Malvinas Current Velocity Structure // Journal of Geophysical Research: Oceans. — 2021. — Vol. 126, no. 4. — https://doi.org/10.1029/2020jc016727.

Garabato A. C. Naveira, Ferrari R. and Polzin K. L. Eddy stirring in the Southern Ocean // Journal of Geophysical Research. — 2011. — Vol. 116, no. C9. — https://doi.org/10.1029/2010jc006818.

GEBCO Bathymetric Compilation Group 2022. The GEBCO_2022 Grid – a continuous terrain model of the global oceans and land. — 2022. — https://doi.org/10.5285/E0F0BB80-AB44-2739-E053-6C86ABC0289C.

Gille S. T., McKee D. C. and Martinson D. G. Temporal changes in the Antarctic circumpolar current: Implications for the Antarctic continental shelves // Oceanography. Special Issue on Ocean-Ice Interaction. — 2016. — Vol. 29, no. 4. — P. 96–105.

Graham R. M., Boer A. M. de, Heywood K. J., et al. Southern Ocean fronts: Controlled by wind or topography? // Journal of Geophysical Research: Oceans. — 2012. — Vol. 117, no. C8. — https://doi.org/10.1029/2012jc007887.

Guide for Chemical Analysis of Marine and Fresh Waters during Ecological Monitoring of Fishery Reservoirs and Regions of the World Ocean, Prospective for Commercial Fishery / ed. by V. V. Sapozhnikov. — Moscow : VNIRO, 2003. — (In Russian).

Intergovernmental Oceanographic Commission. Chemical methods for use in marine environmental monitoring. — UNESCO, 1983. — 53 p.

Karlson B., Cusack C. and Bresnan E. Microscopic and molecular methods for quantitative phytoplankton analysis. — Unesco, 2010. — 110 p. — https://doi.org/10.25607/OBP-1371.

Langlais C., Rintoul S. and Schiller A. Variability and mesoscale activity of the Southern Ocean fronts: Identification of a circumpolar coordinate system // Ocean Modelling. — 2011. — Vol. 39, no. 1/2. — P. 79–96. — https://doi.org/10.1016/j.ocemod.2011.04.010.

Lévy M., Franks P. J. and Smith K. S. The role of submesoscale currents in structuring marine ecosystems // Nature Communications. — 2018. — Vol. 9, no. 1. — P. 4758. — https://doi.org/10.1038/s41467-018-07059-3.

Maslennikov V. V. Climate fluctuations and the Antarctic marine ecosystem: doctoral dissertation. — Moscow : VNIRO, 2004. — EDN: NNIJRJ ; (in Russian).

Maslennikov V. V. and Popkov V. V. Position of the interaction zone of Antarctic waters of various modifications as an indicator of the northern boundary of the mass drift of Antarctic krill // Antarctica: Reports of the Interdepartmental Commission for the Study of Antarctica. Vol. 27. Vol. 27. — Moscow : Nauka, 1988. — P. 134–142. — (In Russian).

Morozov E. G., Frey D. I., Krechik V. A., et al. Multidisciplinary Observations across an Eddy Dipole in the Interaction Zone between Subtropical and Subantarctic Waters in the Southwest Atlantic // Water. — 2022. — Vol. 14, no. 17. — P. 2701. — https://doi.org/10.3390/w14172701.

Murphy J. and Riley A. J. A Single-Solution Method for the Determination of Soluble Phosphate in Sea Water // Journal of the Marine Biological Association of the United Kingdom. — 1958. — Vol. 37, no. 1. — P. 9–14. — https://doi.org/10.1017/s0025315400014776.

Orsi A. H., III T. Whitworth and Jr W. D. Nowlin. On the meridional extent and fronts of the Antarctic Circumpolar Current // Deep Sea Research Part I: Oceanographic Research Papers. — 1995. — Vol. 42, no. 5. — P. 641–673. — https://doi.org/10.1016/0967-0637(95)00021-w.

Palter J. B., Marinov I., Sarmiento J. L., et al. Large-Scale, Persistent Nutrient Fronts of the World Ocean: Impacts on Biogeochemistry // Chemical Oceanography of Frontal Zones. — Springer Berlin Heidelberg, 2013. — P. 25–62. — https://doi.org/10.1007/698_2013_241.

Pujol M. I., Faugére Y., Taburet G., et al. DUACS DT2014: the new multi-mission altimeter data set reprocessed over 20 years // Ocean Science. — 2016. — Vol. 12, no. 5. — P. 1067–1090. — https://doi.org/10.5194/os-12-1067-2016.

Rintoul S. R., Hughes C. W. and Olbers D. Chapter 4.6 The Antarctic circumpolar current system // Ocean Circulation and Climate - Observing and Modelling the Global Ocean. Vol. 77. — Elsevier, 2001. — P. 271–XXXVI. — https://doi.org/10.1016/s0074-6142(01)80124-8.

Sokolov S. and Rintoul S. R. On the relationship between fronts of the Antarctic Circumpolar Current and surface chlorophyll concentrations in the Southern Ocean // Journal of Geophysical Research: Oceans. — 2007. — Vol. 112, no. C7. — https://doi.org/10.1029/2006jc004072.

Sokolov S. and Rintoul S. R. Circumpolar structure and distribution of the Antarctic Circumpolar Current fronts: 1. Mean circumpolar paths // Journal of Geophysical Research: Oceans. — 2009a. — Vol. 114, no. C11. — https://doi.org/10.1029/2008jc005108.

Sokolov S. and Rintoul S. R. Circumpolar structure and distribution of the Antarctic Circumpolar Current fronts: 2. Variability and relationship to sea surface height // Journal of Geophysical Research: Oceans. — 2009b. — Vol. 114, no. C11. — P. 1–15. — https://doi.org/10.1029/2008JC005248.

Stukel M. R., Aluwihare L. I., Barbeau K. A., et al. Mesoscale ocean fronts enhance carbon export due to gravitational sinking and subduction // Proceedings of the National Academy of Sciences. — 2017. — Vol. 114, no. 6. — P. 1252–1257. — https://doi.org/10.1073/pnas.1609435114.

Sun J. and Liu D. Geometric models for calculating cell biovolume and surface area for phytoplankton // Journal of Plankton Research. — 2003. — Vol. 25, no. 11. — P. 1331–1346. — https://doi.org/10.1093/plankt/fbg096.

Tarakanov R. Y. and Gritsenko A. M. Fine-jet structure of the Antarctic Circumpolar Current south of Africa // Oceanology. — 2014. — Vol. 54, no. 6. — P. 677–687. — https://doi.org/10.1134/s0001437014050130.

Thompson A. F., Haynes P. H., Wilson C., et al. Rapid Southern Ocean front transitions in an eddy-resolving ocean GCM // Geophysical Research Letters. — 2010. — Vol. 37, no. 23. — https://doi.org/10.1029/2010GL045386.

Thompson A. F. and Sallée J. B. Jets and Topography: Jet Transitions and the Impact on Transport in the Antarctic Circumpolar Current // Journal of Physical Oceanography. — 2012. — Vol. 42, no. 6. — P. 956–972. — https://doi.org/10.1175/jpo-d-11-0135.1.

Williams R. G., Wilson C. and Hughes C. W. Ocean and Atmosphere Storm Tracks: The Role of Eddy Vorticity Forcing // Journal of Physical Oceanography. — 2007. — Vol. 37, no. 9. — P. 2267–2289. — https://doi.org/10.1175/jpo3120.1.